Biophysical *Journal*
Article

Biophysical Society

Solvatochromic Modeling of Laurdan for Multiple Polarity Analysis of Dihydrosphingomyelin Bilayer

Nozomi Watanabe,[1] Yuka Goto,[1] Keishi Suga,[1] Thomas K. M. Nyholm,[2] J. Peter Slotte,[2] and Hiroshi Umakoshi[1,*]
[1]Graduate School of Engineering Science, Osaka University, Toyonaka, Osaka, Japan and [2]Department of Biochemistry, Faculty of Science and Engineering, Åbo Akademi University, Turku, Finland

ABSTRACT The hydration properties of the interface between lipid bilayers and bulk water are important for determining membrane characteristics. Here, the emission properties of a solvent-sensitive fluorescence probe, 6-lauroyl-2-dimethylamino naphthalene (Laurdan), were evaluated in lipid bilayer systems composed of the sphingolipids D-*erythro*-N-palmitoyl-sphingosylphosphorylcholine (PSM) and D-*erythro*-N-palmitoyl-dihydrosphingomyelin (DHPSM). The glycerophospholipids 1-palmitoyl-2-palmitoyl-*sn*-glycero-3-phosphocholine and 1-oleoyl-2-oleoyl-*sn*-glycero-3-phosphocholine were used as controls. The fluorescence properties of Laurdan in sphingolipid bilayers indicated multiple excited states according to the results obtained from the emission spectra, fluorescence anisotropy, and the center-of-mass spectra during the decay time. Deconvolution of the Laurdan emission spectra into four components based on the solvent model enabled us to identify the varieties of hydration and the configurational states derived from intermolecular hydrogen bonding in sphingolipids. Sphingolipids showed specific, interfacial hydration properties stemming from their intra- and intermolecular hydrogen bonds. Particularly, the Laurdan in DHPSM revealed more hydrated properties compared to PSM, even though DHPSM has a higher T_m than PSM. Because DHPSM forms hydrogen bonds with water molecules (in 2NH configurational functional groups), the interfacial region of the DHPSM bilayer was expected to be in a highly polar environment. The careful analysis of Laurdan emission spectra through the four-component deconvolution in this study provides important insights for understanding the multiple polarity in the lipid membrane.

INTRODUCTION

Plasma membrane bilayers play a fundamental role in regulating cellular function by delineating a membrane wall that divides the intracellular and extracellular spaces. In addition, each function of the membrane—such as encapsulation, localization of proteins, and molecular permeation across the membrane—depends on the compositions of their membrane proteins and lipid species (1). The integration of external (or internal) biomolecules into the membrane surface is promoted by several factors; the electrostatic and hydrophobic interactions between those molecules and the membranes are usually dominant (2–4). Furthermore, the water molecules at the interface of the lipid membrane can control the activities of biomolecules by modulating the surface pressure, coordination of hydrogen bonding, and surface charge state (5–9). Lipid rafts, usually composed of sphingolipids and cholesterol, have been attracting research attention for many years because of their functional interaction with biomolecules (10–14). In the lipid raft, the membrane interface could be maintained in a less hydrated state because of the rigid and ordered alignments of lipid molecules, which can exclude the water molecules. Therefore, the membrane polarity in the lipid raft is thought to play an important role in the integration of molecules or the control of their activity. However, little is known regarding the interfacial hydration state of local raft regions compared to other regions within the same membrane because the observation methodology of heterogenic hydration properties has not been well established.

Sphingolipids are the major lipid species known to be associated with raft domain stability (15). They form a strong intermolecular hydrogen bond that facilitates the segregation with high affinity to cholesterol through the hydrogen-bonding acceptor (C=O, P=O, 3OH, or 2NH) and donor moieties (3OH or 2NH) (14,16). Most sphingolipids have a long, saturated acyl chain, which allows them to be packed tightly (17). Even with a subtle configurational difference of saturated or unsaturated, the physicochemical properties, such as the phase transition temperature (T_m) of sphingolipids in bilayers, can vary.

Submitted August 13, 2018, and accepted for publication January 28, 2019.
*Correspondence: umakoshi@cheng.es.osaka-u.ac.jp
Editor: Georg Pabst.
https://doi.org/10.1016/j.bpj.2019.01.030

For example, D-*erythro*-N-palmitoyl-sphingosylphosphorylcholine (PSM), having a saturated acyl chain and an unsaturated long-chain base, shows a T_m of 41.2°C in the its pure bilayer form (18). D-*erythro*-N-palmitoyl-dihydrosphingomyelin (DHPSM), having a saturated long-chain base, shows a T_m of 47.7°C in its bilayer form (19–21). The former and later sphingolipids are a predominant species in most plasma cell membranes and in human lens cell membranes, respectively. Recent studies have reported differences in their hydrogen-bonding properties (19,22). Dihydrosphingomyelin (dihydro-SM) is assumed to have higher affinity for cholesterol than unsaturated SM. It is clear that the molecular environments arranged via hydrogen bonds are specific; therefore, microscopic properties, such as membrane polarity or viscosity between the lipid molecules, should be properly verified.

The fluorescence probe 6-lauroyl-2-dimethylamino naphthalene (Laurdan) has been widely used to evaluate membrane hydration states (23–25). The fluorescence emission of Laurdan is sensitive to the surrounding solvent environment. In the lipid bilayer, the amphipathic structure of Laurdan localizes it at the hydrophobic-hydrophilic interface region. Thus, the obtained information is relevant to the microscopic interfacial properties of the lipid bilayer (25,26). Through excitation, the fluorophore moiety has a large dipole moment (26,27) and exhibits various emission characteristics relaxed by the surrounding solvent molecules (25,28,29). An analytical method for measuring the microscopic polarity of the membrane has been developed by utilizing the emission properties of Laurdan in the lipid bilayer (26,30–32); for the two-state assumption of membrane phase state (gel phase or liquid phase), the generalized polarization (*GP*) value is widely used (23,29,33). Despite this versatility, further investigation is required to evaluate various hydration states at the lipid bilayer interface, as there are many factors that would affect the heterogeneity of Laurdan relaxation (e.g., hydrogen bonding, lateral lipid density, and lateral heterogeneity) (33). One example is the broad emission spectra of the Laurdan found in the sphingolipid bilayer (20,25,34); however, from where it originates is unclear, aside from the possibility of intermolecular hydrogen bonds among sphingolipids.

In this study, we evaluated the interfacial hydration properties of bilayers prepared from different lipid species to determine whether the different configurations, including backbone structure or degree of saturation, affect the interfacial hydration properties of the bilayers. Specifically, we focused on how the hydrogen-bonding properties of PSM and DHPSM affected the interfacial polarity. The steady-state measurements of the excitation spectra and emission spectra and the anisotropy of Laurdan were carefully investigated along with the time-resolved emission analysis. Here, we propose the deconvolution of obtained Laurdan fluorescence emission spectra into four components based on the emission properties of the solvent system. The differences in the microscopic polar environments arranged in each lipid bilayer were discussed in this study based on the "solvatochromic model" of Laurdan, in which its local surroundings are assigned as a solvent system.

MATERIALS AND METHODS

Materials

Phospholipids (1-palmitoyl-2-palmitoyl-*sn*-glycero-3-phosphocholine (DPPC), and 1-oleoyl-2-oleoyl-*sn*-glycero-3-phosphocholine (DOPC)) and egg yolk SM were purchased from Avanti Polar Lipids (Alabaster, AL). PSM was purified from egg yolk SM, as described previously (20). PSM was hydrogenated to yield DHPSM, as previously reported (17). The purity of the SMs was confirmed by mass spectrometry. Laurdan was purchased from Sigma Aldrich (St. Louis, MO). Other chemicals were obtained from Wako Pure Chemical Industries (Osaka, Japan) and used without further purification.

Preparation of the lipid bilayer vesicles

Lipids and fluorescence probes were dissolved in methanol. Appropriate amounts were dispensed into glass tubes, and the solvent was evaporated under a stream of nitrogen gas. The dry lipid films were hydrated in pure water at 65°C (60 min) and sonicated in a sonicator bath (Bransonic 2510; Branson Ultrasonics, Danbury, CT), for 5 min at 65°C. Large unilamellar vesicles (100 nm in diameter) were prepared by extrusion at 65°C (35). The lipid concentration was measured using the method reported by Rouser et al. (36).

Fluorescence measurements of Laurdan in steady state

All samples were prepared to adjust the final lipid and Laurdan concentrations to 100 and 1 μM, respectively. The concentration of Laurdan was estimated from its absorbance using the molecular extinction coefficient (ε = 2000 cm^{-1}) (37). Steady-state fluorescence measurements were performed with a QuantaMaster (Photon Technologies International, Lawrenceville, NJ). The temperature of the sample cell was monitored and regulated by a Peltier system, and data acquisition was controlled using Felix 32 software. Emission measurements were performed using excitation light at 360 nm, and the emission spectra of Laurdan were collected from 400 to 540 nm.

Fluorescence anisotropy, *r*, was calculated from vertically and horizontally polarized emission intensity with the following equations:

$$r = (I_{VV} - GI_{VH})/(I_{VV} + 2GI_{VH}) \quad (1)$$

$$G = I_{HV}/I_{HH} \quad (2)$$

where the orientation of the excitation and emission polarizers were represented as follows, for example, I_{HV} for the intensity horizontally polarized excitation and vertically polarized emission, as defined in a previous report (38). The changes of anisotropy as a function of temperature were continuously measured from 20 to 70°C, and the results were analyzed with the sigmoidal fitting curves, based on Boltzmann equation. The measurement was performed using excitation light at 360 nm, and the emission was measured at 490 nm.

The deconvolution of obtained emission spectra was carried out using PeakFit software (Systat Software, San Jose, CA). All fitting equations were utilized with the lognormal amplitude function following a previous report (31). The equation for the fitting is as follows:

$$y = a_0 exp\left(-\frac{1}{2}\left(\frac{\ln\frac{x}{a_1}}{a_2}\right)^2\right) \quad (3)$$

where a_0 is the amplitude, a_1 is the center ($\neq 0$), and a_2 is the width (>0) of the fitting curve, respectively. From the fitting acquisition, the integrated area and its area ratio [%] were obtained; the integrated area was calculated from the integration of the obtained analytical curve.

Time-resolved fluorescence measurements

Time-resolved fluorescence measurements were all performed using the FluoTime 200 instrument (PicoQuant, Berlin, Germany). The sample temperature was controlled by a Peltier system, and data acquisition was performed with the PicoHarp system. The samples were excited with a 378-nm diode laser, and the emission was measured from 400 to 540 nm in 10-nm steps (14 acquisitions). The time resolution was 64 ps. A decay curve was produced after 150 s of acquisition time. Data were analyzed using FluoFit Pro software. After integration of all decay curves, the time-resolved emission spectra were extracted every 1.6 ns after excitation (from 7.168 to 48.768 ns, in 28 spectra), and the center of spectral mass (λ) was calculated according to a previous report as follows (39):

$$\lambda = \sum \lambda_i F_i \Big/ \sum F_i \quad (4)$$

where F_i is the fluorescence emitted at the emission wavelength λ_i.

RESULTS

Emission spectra of Laurdan in the steady state

The fluorescence emission spectra of Laurdan were measured in the bilayers composed of DPPC, DOPC, PSM, and DHPSM. As shown in Fig. 1, the Laurdan in the DPPC bilayer (T_m: 41.2°C) showed a sharp peak at around 440 nm, which was consistent with the reported Laurdan peak position in the gel phase bilayer (23). The Laurdan spectrum in the DOPC bilayer showed a broader and red-shifted peak at ~490 nm, which was derived from the Laurdan in the liquid-crystalline phase. For the PSM and DHPSM bilayers, broader peaks were observed compared with the spectrum in the DPPC bilayer. These findings are similar to previous results (20), whereas narrower and blue-shifted peaks were observed in this study because of the lower experimental temperature (at 20°C). The phase transition temperatures of PSM and DHPSM in the bilayers were 41.2 and 47.7°C, respectively (18). At the point that these lipid bilayers have a high T_m, it is expected that the membrane properties of PSM and DHPSM bilayers could be similar and resemble that of the DPPC bilayer. However, broader peaks at 440 nm in PSM and at 460 nm in DHPSM were observed. Furthermore, the spectrum in the DHPSM bilayer was more red-shifted than in the PSM bilayer and seemed to be considerably similar to that in the DOPC bilayer. These results suggest that the

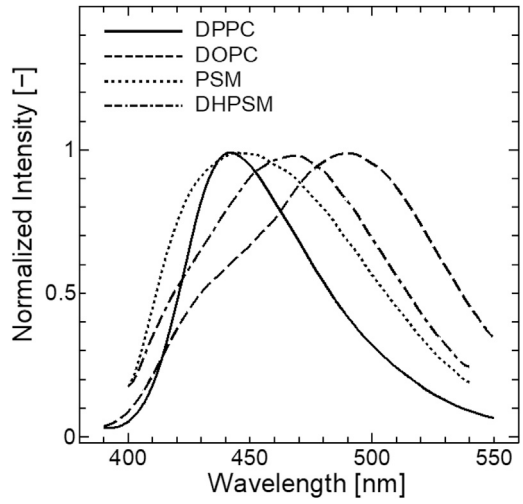

FIGURE 1 Fluorescence emission spectra of Laurdan in DPPC (*solid*), DOPC (*dash*), PSM (*dot*), and DHPSM (*dot 2-dash*) bilayers at 20°C. The excitation wavelength was 360 nm. All spectra were normalized with the strongest peak intensity. The reproducibility found from the different compositional binary systems is also shown in Fig. S1.

Laurdan in SM bilayers would be in multiple hydration states, and it may be highly hydrated in the DHPSM bilayer. Conventional *GP* analysis was also attempted (Fig. S2). The *GP* values of the SM bilayers below the T_m were relatively low, in the order of DOPC < DHPSM < PSM < DPPC, which implies that the order of hydrophobicity does not correspond to the rigidity expected from the T_m.

Anisotropy of Laurdan

The rotational mobility of the fluorescent molecules in the bilayers was investigated using steady-state anisotropy (Fig. 2). The anisotropy values decrease during phase transition, wherein the rotational mobility or molecular freedom increase. In the DPPC bilayer, a drastic shift in the anisotropy was observed at T_m (= 41°C). Because the DOPC bilayer is in a fluid and disordered state, there was only a slight decrease. The PSM and DHPSM bilayers showed modestly shifted anisotropy values compared to the shift observed in the DPPC bilayer systems. Further, at temperatures below T_m, the anisotropy values in SM bilayers were slightly lower than in the DPPC bilayer. These results indicate that there are some configurational factors in SM bilayers, for example, the high saturation of hydration or hydrogen bonding, and that they restrict Laurdan to having a modest transition of rotational motion as the temperature increases.

The anisotropy transition was dependent on the emission wavelength, and at shorter emission wavelengths, a modest shift was observed in the results of the DPPC bilayer. Anisotropy dependencies on the emission wavelength can be explained by the existence of individual molecular species that have different emission properties. For the phase

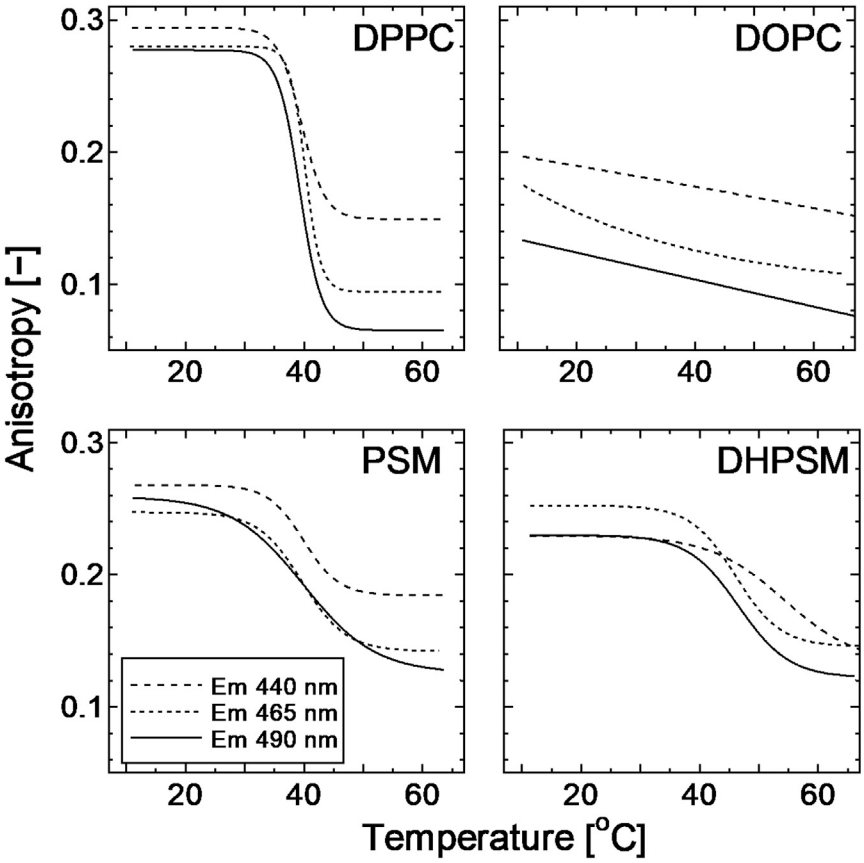

FIGURE 2 Anisotropy transitions of Laurdan in DPPC, DOPC, PSM, and DHPSM bilayers as a function of temperature. The excitation wavelength was 360 nm, and the emission wavelength was at 440 nm (*dashed line*), 465 nm (*dotted line*), and 490 nm (*solid line*). Anisotropy was calculated using Eqs. 1 and 2. The sigmoidal fitting curve was illustrated using the Boltzmann equation. The reproducibility found from the different compositional binary system is also shown in Fig. S3.

transition of DHPSM bilayers, the anisotropies with the longer emission wavelengths (465 and 490 nm) shifted at a lower temperature than the one at a shorter emission wavelength (440 nm), suggesting that Laurdan molecules with longer wavelength emissions have high mobility or heat sensitivity. The results shown in Figure S4 indicate the fluorescence quenching by the radical reagents (5-DOXYL stearic acid; 2-(3-carboxypropyl)4,4-dimethyl-2-tridecyl-3-oxazolidinyloxy (lipophilic) and 2,2,6,6-tetramethylpiperidine 1-oxyl (water soluble)) located at the interfacial region. The significant quenching in the longer wavelength range was observed in SM bilayers, which implies that the Laurdan molecules with red emission are locating in the shallower region of the interface. This also supports the idea of various locations of Laurdan with corresponding polarities.

Center of mass of the time-resolved emission spectra

The center of mass of the time-resolved emission spectrum of Laurdan was calculated for the DPPC, DOPC, PSM, and DHPSM bilayers (Fig. 3). In general, slow dipolar relaxation around the excited state of the probe makes fluorophores emit earlier with higher energy (shorter wavelength), whereas fast dipolar relaxation leads to a loss of energy due to environmental relaxation (higher wavelength). For the DPPC bilayer below T_m, a small shift of the center of mass was observed with decay time, which confirms the gel phase as reported previously (30,40). The center of mass in the DOPC bilayer shifted to a larger emission wavelength and returned to a shorter wavelength because the dynamic solvent relaxation in the liquid-crystalline phase resulted in a red-shifted emission and a short lifetime. With regard to the temperature effect found in the DOPC bilayer, a progressive red shift and shorter decay time were observed at high temperature, indicating that significant solvent relaxation from the surrounding hydrated waters makes the lifetime of Laurdan shorter. Similar tendencies were also observed in DPPC bilayers at temperatures above T_m. A unique feature of sphingolipids was that the center of mass shifted to a large wavelength with a shorter decay time. This result is similar to the property observed in the liquid-crystalline phase, although the degree of red shifting was modest compared to that in the DOPC bilayer. This suggests that there are specific molecular arrangements among sphingolipids that enable Laurdan to be relaxed. Further, the transition of the center of mass in the DHPSM bilayer at a low temperature was more red-shifted compared with those in the PSM bilayers, again indicating the highly hydrated property of the DHPSM bilayer. Considering the biphasic time distributions of center-of-mass values in DOPC and SM bilayers, there

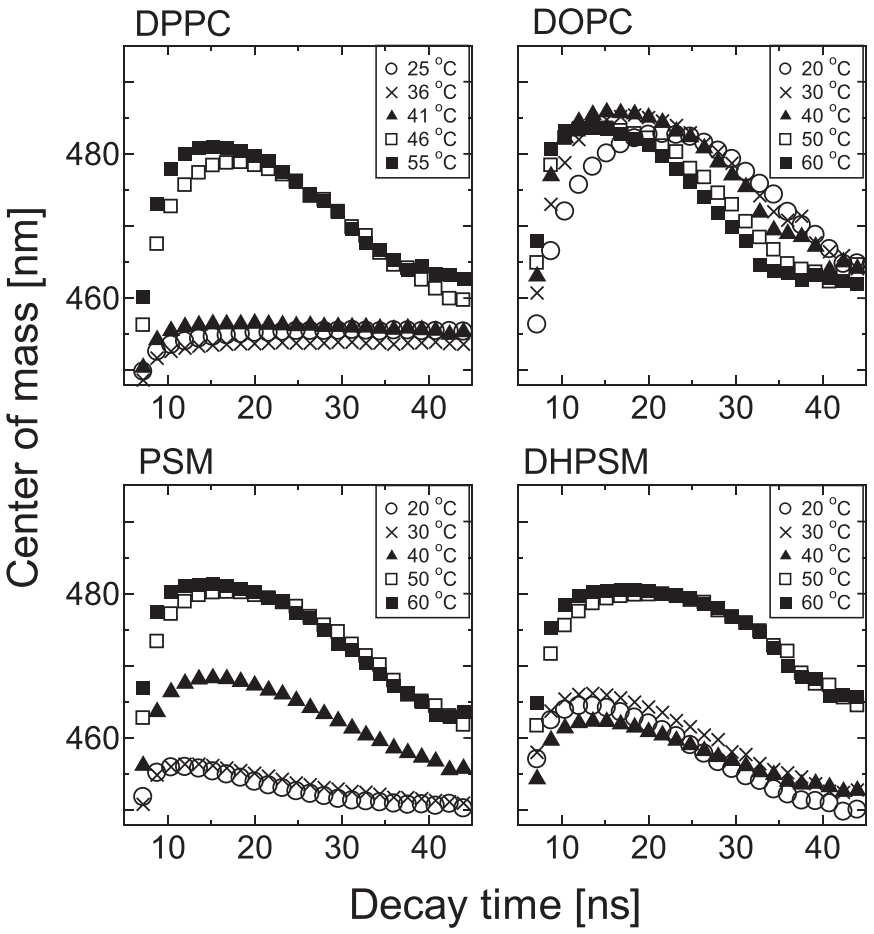

FIGURE 3 The center of mass of the time-resolved spectra of Laurdan for each bilayer at different temperatures. The excitation wavelength for the diode laser was 378 nm. The value of the center of mass was calculated using Eq. 4. Each data point was extracted every 7.168 ns. The reproducibility found from the different compositional binary system is also shown in Fig. S5.

could be at least two populations of fluorophores emitting at the shorter wavelengths: one with short lifetimes and one with long lifetimes.

Excitation spectrum of Laurdan

Fig. 4 shows the excitation spectra of Laurdan in each lipid bilayer for the emission wavelengths 435 and 470 nm. According to a previous report, the specific intermolecular interactions between Laurdan and the surrounding molecules can be determined from excitation spectra (25). The emission wavelength dependencies at 435 and 470 nm were significant for both SM bilayers. Greater blue-edge excitation intensity was found in the DOPC bilayer and SM bilayers. The excitation peaks with shorter wavelength could indicate energetically unfavorable states of Laurdan species, for example, one in the fluid membrane wherein the quantum yield of Laurdan is relatively low (25,40,41). In addition, the Laurdan in nonpolar (low dielectric constant (ε)) and aprotic solvent emits rather weak fluorescence (42). Therefore, it seems that a portion of the Laurdan molecules in the DOPC and SM bilayers are energetically unfavorable because of high fluidity or low ε. The excitation spectra for the emission wavelength of 470 nm showed a decreased blue-edge intensity, revealing the different locations of Laurdan molecules depending on the emission wavelength. This increased red-edge intensity implies the presence of relaxation. The spectra in the DHPSM bilayer had relatively larger red-edge intensities than in the PSM bilayer, suggesting that the intermolecular interaction between Laurdan and the solvent molecules is greater in the DHPSM bilayer.

The emission ratio spectra based on the different excitation wavelengths are shown in Fig. S7. When the fluorescence molecules are excited with longer wavelengths, the intensity of the blue-edge emission decreases because the photo selection occurs for molecules that are already relaxed and energetically favorable (25). The emission spectra obtained with red excitation for the DOPC and DHPSM bilayers showed lower intensities of blue-edge emission at 25°C, indicating that relaxation is taking place. In the DPPC, PSM, and DHPSM bilayers, spectra with blue excitation (340 nm) showed greater intensity in the blue-edge emission above T_m (60°C), which implies the existence of energetically unrelaxed molecules after the phase transition. These results indicate the unique heterogeneity of Laurdan in the DHPSM bilayer, which can sense both hydrophilic and hydrophobic environments.

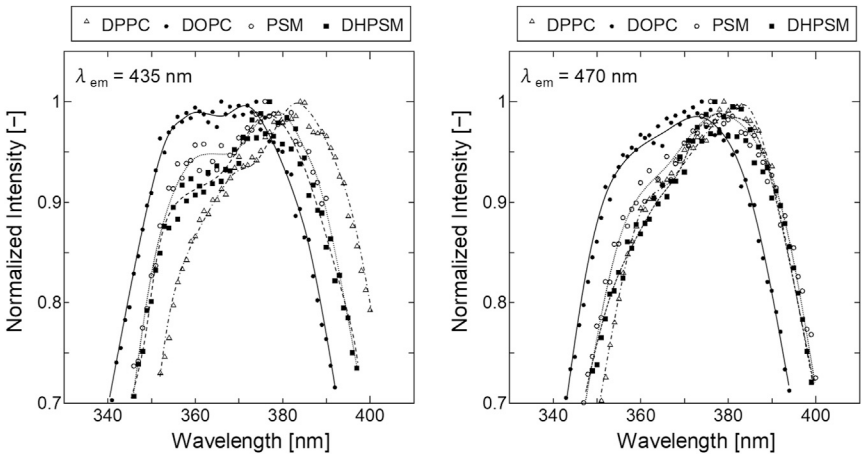

FIGURE 4 Laurdan excitation spectra of pure lipid bilayers at emission wavelength (λ_{em} = 435, 470 nm) in 20°C. The symbols indicate the type of lipid bilayer: DPPC (*open triangle*), DOPC (*closed circle*), PSM (*open circle*), and DHPSM (*closed square*). All spectra were normalized with the strongest peak intensity. The Laurdan excitation spectra of binary systems (DOPC/PSM, DOPC/DHPSM) are also shown in Fig. S6. The spectral differences are found in our experiments compared with previous report are considered to originate from the difference of purity of the lipids (between extracted SM and purified SM).

DISCUSSION

Interpretation of hydration states in PC and SM bilayers using the fluorescence properties of Laurdan

Analysis of the Laurdan fluorescence is a useful tool for characterizing membrane interfaces. However, it is difficult to interpret its complex molecular environment. In this study, the fluorescence properties were observed according to the emission wavelengths; for example, a modest shift in the anisotropy at a shorter emission wavelength (Fig. 2), a shorter lifetime at a longer emission wavelength (Fig. 3), and a larger red-edge intensity of the excitation spectra at a longer emission wavelength (Fig. 4). In particular, the properties of Laurdan in PSM and DHPSM bilayers revealed the complexities for the interpretation, as suggested by the broad and decomposable emission peak (Fig. 1), the significant quenching in the red-edge emission (Fig. S4), the unique red shift of the center of mass (Fig. 3), and the emission dependence on the excitation spectra (Fig. 4). This complexity is caused by a variety of excited states and the diversity of the probe's surroundings (microscopic viscosity, hydration degree, and so on) (29,33). Because of this complexity, common *GP* analysis often encounters discrepancies in terms of the selection of blue and red peaks (33). Moreover, deconvolution analysis with the double component cannot precisely account for the molecular situation (31).

Here, the multiple deconvolution analysis based on the solvent system was used to examine the correlation between the Laurdan emission peaks and the dielectric constants of the solvents. Because the local dielectric constant (ε) of the bilayer membrane drastically shifted from 10 to 70, the solvent property in the bilayer should be studied carefully (43). The local solvent characteristic could be explained by separately considering molecular environments as featured solvent systems, such as nonpolar ($\varepsilon < 5$), polar aprotic, polar protic (low ε), and polar protic (high ε) systems. The characterization of polar protic solvent can be divided into low and high ε to explain the protic effect of both the water molecules penetrating the hydrophobic region of the membrane and the abundance of water molecules in the polar region. Based upon this assumption, a series of solvent mixtures were selected to represent the molecular environments, such as the hexane-acetone system (ε: 1.89 $\sim$ 20.7) for the effect of the C=O group, the hexane-ethanol (ε: 1.89 $\sim$ 24.5) for the protic effect in the hydrophobic region, and ethanol-water (ε: 24.5 $\sim$ 80.1) for the water-abundant region.

The deconvolution results of the three solvent mixture systems are shown in the Supporting Materials and Methods (see "Deconvolution Analysis and the Solvent Model"). In the ε region corresponding to the membrane interface, the correlations of the peak positions were observed: less than 440 nm for the nonpolar solvent, 440 $\sim$ 460 nm for the polar aprotic, 460 $\sim$ 480 nm for the polar protic with low ε, and greater than 480 nm for the polar protic with high ε, respectively. Because the emission range of the Laurdan spectra in the lipid bilayer is broad enough to cover the entire range, it is possible to assign these four solvent systems to the multiple deconvolution curves (as performed in the next section). A more in-depth explanation of the deconvolution analysis is provided in the Supporting Materials and Methods.

Deconvolution of the Laurdan spectra

Fig. 5 shows the peak positions and the area ratios obtained from the four deconvolution curves with good correlation coefficient (for details, see Fig. S8). Based on the solvent models (Fig. S9–S11; Scheme 1 in the Supporting Materials and Methods), they can be classified into four groups. In the DPPC, PSM, and DHPSM bilayers, the most blue-shifted peak at ~420 nm disappeared during the phase transition. This peak originates from Laurdan existing in the nonpolar region (i.e., a tightly packed alignment or hydrogen bond interactions could prevent the solvation into fluorophores). Interestingly, in the loosely packed bilayers (such

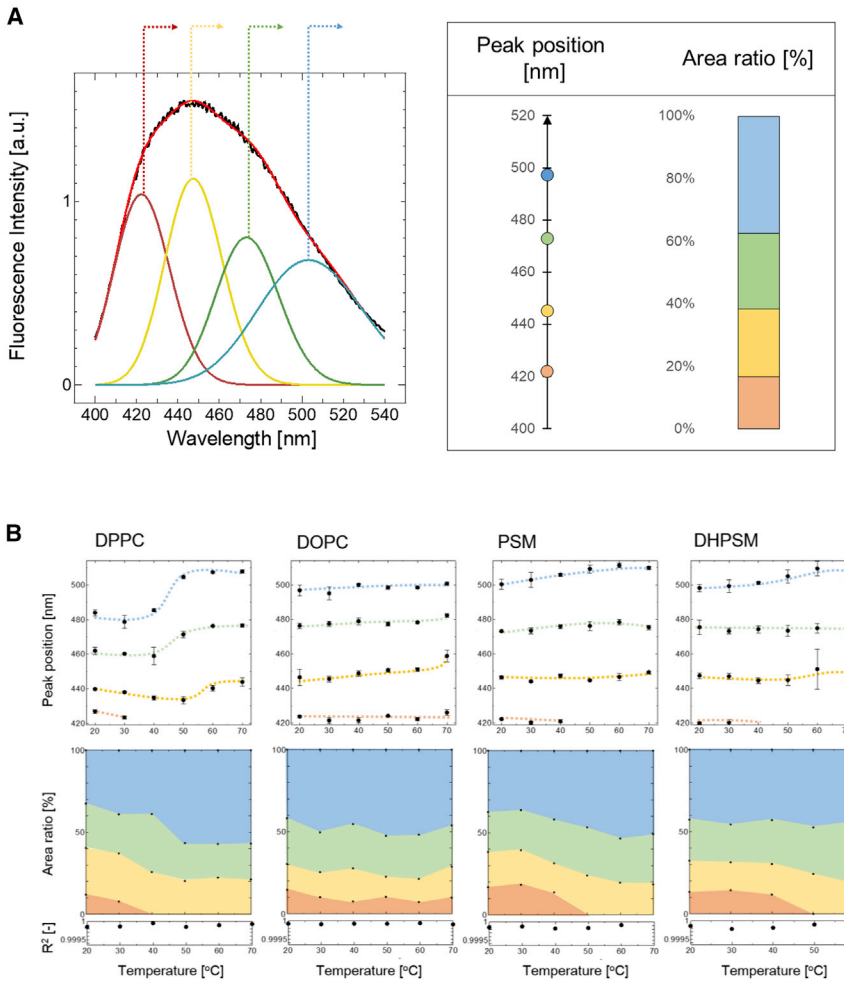

FIGURE 5 (*A*) Deconvoluted emission spectra of Laurdan using the lognormal fitting function as described in Eq. 3. From the four deconvolution curves, the peak positions of curves and integrated area ratios toward the whole spectral area were calculated. The peak position and integrated area percentage obtained from each bilayer were pictured in the corresponding color with the deconvolution spectra. (*B*, *upper*) The peak positions of deconvolution curves as a function of temperature, in DPPC, DOPC, PSM, and DHPSM bilayers, are shown. (*B*, *lower*) The transition of area ratios of deconvolution curves as a function of temperature is shown. To see this figure in color, go online.

as DOPC), Laurdan also had a peak at 420 nm throughout the whole temperature range. This result seems contradictory. However, the Laurdan in the DOPC bilayer had a short lifetime (~2 ns) at an emission of 420 nm (data not shown), suggesting that the blue-shifted components in DOPC bilayers are observable but energetically unfavorable because of collisional effects. As shown in the results of center of mass (Fig. 3), DOPC and SM bilayers indicated at least two populations of fluorophores emitting at the shorter wavelengths with short and long lifetimes. In a dynamic solvent environment, the quantum yield of Laurdan is relatively low, which means some of the excited Laurdan could be immediately brought back to the ground state through the nonradiative pathway (38). Compared with other bilayers, lower anisotropy values at the blue-shifted region (at 440 nm) in DOPC bilayers were shown, which also suggests a different fluorescence nature with high molecular motility in DOPC bilayers (Fig. 2). Low viscosity makes the fluorescence lifetime shorter (41). Therefore, the blue-edge emission in DOPC bilayer is considered to be significant with short-lifetime components in high mobility; on the other hand, the blue-edge emission in SM bilayers is expected to be significant, with long-lifetime components with high viscosity in a nonpolar environment in the tightly packed membrane state. The peak component with the largest emission peak (at around 500 nm) corresponded to the polar protic solvent model with the highest ε value (Fig. S10). In the solvent systems, the presence of more than 60% water (over ε ~30) decreased the emission intensity, whereas the blue-edge excitation increased. This means that Laurdan can acquire unfavorable energy states in a high polar environment. Studies using theoretical calculation and an electrostatic force microscope reported dielectric constants around the polar region of ε ~30 (44,45). Therefore, the environment with the highest dielectric constants detected by Laurdan was ~30, and Laurdan could be located in the shallower polar region of the membrane.

Compared with the deconvolution curve in the DPPC bilayer, those in the PSM and DHPSM bilayers resulted in more red-shifted peaks similar to the result in the DOPC bilayer. In the DPPC bilayer, a shift in the peak position during the phase transition was observed; however, in the SM bilayers, the red shifts were minor. These results indicate that the Laurdan molecules in SM bilayers could be

distributed heterogeneously; one could be positioned in a significantly hydrated polar protic region similar to that in a DOPC bilayer, and the other could be placed in a less hydrated nonpolar region than that in a DPPC bilayer. The existence of the nonpolar components in SM bilayers was also confirmed by the increase in the blue-edge intensity of the excitation spectra at an emission of 435 nm (Fig. 4).

Hydrogen-bonding network and interfacial hydration states in SMs

According to previous studies of PSM and DHPSM bilayers, DHPSM bilayers have stronger intermolecular hydrogen networks than PSM, which could be one of the possible reasons explaining the differences in their physicochemical properties in the bilayers, as mentioned previously ($T_{m,\ PSM}$; 41.2°C < $T_{m,\ DHPSM}$; 47.7°C) (46,47). The immiscibility of the dihydro-stearoyl-SM and DOPC bilayers was attributed to strong intermolecular hydrogen bonding in dihydro-SM (48). Therefore, the structure of the DHPSM bilayer is assumed to be highly ordered and less hydrated than that of the PSM bilayer. However, our results revealed highly hydrated properties for the DHPSM bilayer (Figs. 1, 3, 4, and S7) as well as the predominant existence of nonpolar components in the PSM bilayer (Figs. 1, 4, 5, and S4), which appears to be contradictory to the expectations according to the previous observations (46–48).

Yasuda et al. have suggested that DHPSM has a more flexible headgroup compared to PSM based on the quantum chemistry approach (22). They found that the properties of the 3OH group of DHPSM are different than those of PSM because the *trans* double bond in PSM could restrict the rotational motion of the C-C bond when the 3OH group is present. The intramolecular hydrogen bond between the 3OH group and phosphate oxygen is stronger in the PSM than in the DHPSM bilayer, as previously reported (39). The restriction of the 3OH group in PSM influences strong intramolecular hydrogen bonds, and the flexible 3OH group in DHPSM has more opportunities to form hydrogen bonds with other functional groups. PSM has a kinked structure because of the strong intramolecular hydrogen bonds, which prevents PSM molecules from coming close to each other. Hence, the 2NH group of DHPSM exhibits stronger intermolecular interaction via the lipid-water-lipid link than in PSM (47). As shown by the 2,2,6,6-tetramethylpiperidine 1-oxyl quenching experiments (Fig. S4), DHPSM bilayers had more resistance to quenching compared with the PSM bilayer. This indicates that the strong intermolecular interaction in the DHPSM bilayer prevents the penetration of large molecules, such as the quencher molecules.

Thus, it is assumed that DHPSM has enhanced possibilities to form hydrogen bonds, which can stabilize the water molecules around the interfacial region of the lipid bilayer. Based on the previous findings, the water exposure of lipids increases in the following order: PSM < DPPC < DHPSM, as measured from the fluorescence lifetime values of dansyl-PE under the collisional quenching effect of D_2O (20). This also explains the highly dielectric environment at the interface of the DHPSM bilayer and the low accessibility of water into the PSM bilayer.

Plausible model of hydration properties in PC and SM bilayers

A brief model of the membrane hydration and different populations of Laurdan below T_m is illustrated in Fig. 6. Laurdan molecules could be in different solvent environments according to the emission wavelength. Based on our findings, it is expected that Laurdan with longer emission wavelengths is located in a shallower position in the bilayer membrane. The red-edge emission components in the SM bilayers indicate a polar protic environment. It seems that the specific properties of sphingolipids have hydrogen acceptor and donor impacts on hydration behavior. Especially, highly hydrated states were observed in the DHPSM bilayer. The ability of the DHPSM bilayer to retain water molecules is due to the strong intermolecular hydrogen bonds via water bridges. The kinked structure of PSM makes it difficult for intermolecular hydrogen bonds to form with water molecules compared with DHPSM, which also explains the greater ratio of nonpolar components in the PSM bilayer. Generally, the dipole moment of the lipid headgroup derived from the zwitterionic part of the phosphocholine is aligned almost in parallel to the horizontal direction of the bilayer (49–51). It is therefore expected that the Laurdan in the DPPC bilayer will be located in a deeper place in the gel phase membrane. However, a blue-edge excitation spectrum at 435 nm was not found in DPPC (Fig. 4), suggesting that DPPC molecules could not acquire the distribution of Laurdan into nonpolar environment as in

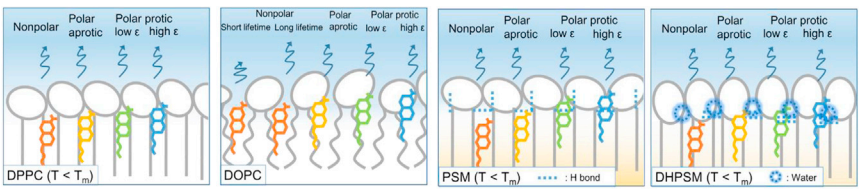

FIGURE 6 Hydration and the molecular model relation between lipid and Laurdan in DPPC, DOPC, PSM, and DHPSM bilayers. Lipids and illustrated in the color of gray. The colors of the Laurdan are illustrated with the corresponding color in Fig. 5; orange for the nonpolar, yellow for the polar aprotic, green for the polar protic with low ε, blue for the polar protic with high ε. The molecular situation for the above T_m is illustrated in Fig. S12. To see this figure in color, go online.

SM bilayers. In the DOPC bilayers, the blue-edge emission component could be unfavorable with a short lifetime because of the surrounding high collisional effect. The long-lifetime component at the blue-edge emission in DOPC bilayer is also existence, hence, both short- and long-lifetime species are illustrated. In SM molecules, the contribution of long lifetime was significant compared with short lifetime at the blue-edge emission, and thus, the long-lifetime species was illustrated as the nonpolar component. Their hydrogen bond donor/acceptor groups could allow the Laurdan to be incorporated into a much deeper place without solvent waters, resultinh in the deconvolution peak components of 420 nm (nonpolar environment). Such a hydrophobic environment in sphingolipids may attribute to a high affinity for hydrophobic cholesterol molecules.

Though these are plausible models, the unique approach in this study provides novel insights, to our knowledge, into the multiple membrane polarity of SM bilayers, which leads us to a much deeper understanding of intermolecular lipid interactions and membrane surface hydration.

SUPPORTING MATERIAL

Supporting Materials and Methods and 12 figures are available at http://www.biophysj.org/biophysj/supplemental/S0006-3495(19)30080-3.

AUTHOR CONTRIBUTIONS

N.W., K.S., J.P.S., and H.U. designed the research. T.K.M.N. and J.P.S. provided the analytical tools. N.W., Y.G., K.S., and T.K.M.N. performed the experiments and analyzed the data. N.W., K.S., T.K.M.N., J.P.S., and H.U. wrote the article.

ACKNOWLEDGMENTS

This work was primarily supported by the Japan Society for the Promotion of Science KAKENHI Grant-in-Aids for Scientific Research (A) (26249116), Grant-in-Aids for Young Scientists (B) (16K18279), and Grant-in-Aids for Challenging Exploratory Research (T15K142040). N.W. expresses her gratitude for a Japan Society for the Promotion of Science Research Fellowship (JP18J11666) and Tobitate! (Leap for Tomorrow) Young Ambassador Program. The Slotte laboratory was supported by generous funds from the Sigrid Juselius Foundation.

SUPPORTING CITATIONS

References (52–58) appear in the Supporting Material.

REFERENCES

1. Luckey, M. 2012. Membrane Structural Biology with Biochemical and Biophysical Foundations. Cambridge University Press, Cambridge, UK.
2. Alberts, B., A. Johnson, …, P. Walter. 2014. Molecular Biology of the Cell, Sixth Edition. Garland Science, New York.
3. Jin, Z. X., C. R. Huang, …, H. Umehara. 2008. Impaired TCR signaling through dysfunction of lipid rafts in sphingomyelin synthase 1 (SMS1)-knockdown T cells. *Int. Immunol.* 20:1427–1437.
4. Villar, V. A., S. Cuevas, …, P. A. Jose. 2016. Localization and signaling of GPCRs in lipid rafts. *Methods Cell Biol.* 132:3–23.
5. Costard, R., I. A. Heisler, and T. Elsaesser. 2014. Structural dynamics of hydrated phospholipid surfaces probed by ultrafast 2D spectroscopy of phosphate vibrations. *J. Phys. Chem. Lett.* 5:506–511.
6. Damodaran, S. 1998. Water activity at interfaces and its role in regulation of interfacial enzymes: a hypothesis. *Colloids Surf. B Biointerfaces.* 11:231–237.
7. Saito, H., and W. Shinoda. 2011. Cholesterol effect on water permeability through DPPC and PSM lipid bilayers: a molecular dynamics study. *J. Phys. Chem. B.* 115:15241–15250.
8. Alarcón, L. M., M. de Los Angeles Frías, …, E. Anibal Disalvo. 2016. Water populations in restricted environments of lipid membrane interphases. *Eur Phys. J. E Soft Matter.* 39:94.
9. Sparr, E., and H. Wennerström. 2001. Responding phospholipid membranes–interplay between hydration and permeability. *Biophys. J.* 81:1014–1028.
10. Simons, K., and E. Ikonen. 1997. Functional rafts in cell membranes. *Nature.* 387:569–572.
11. Barenholz, Y. 2004. Sphingomyelin and cholesterol: from membrane biophysics and rafts to potential medical applications. Membrane Dynamics and Domains. Springer.
12. Casem, M. L. 2016. Membranes and membrane transport. In Case Studies in Cell Biology, M. L. Casem, ed. (Academic Press).
13. Lajoie, P., and I. R. Nabi. 2010. Lipid rafts, caveolae, and their endocytosis. *Int. Rev. Cell Mol. Biol.* 282:135–163.
14. Slotte, J. P. 2016. The importance of hydrogen bonding in sphingomyelin's membrane interactions with co-lipids. *Biochim. Biophys. Acta.* 1858:304–310.
15. Ramstedt, B., and J. P. Slotte. 2002. Membrane properties of sphingomyelins. *FEBS Lett.* 531:33–37.
16. Venable, R. M., A. J. Sodt, …, J. B. Klauda. 2014. CHARMM all-atom additive force field for sphingomyelin: elucidation of hydrogen bonding and of positive curvature. *Biophys. J.* 107:134–145.
17. Ramstedt, B., and J. P. Slotte. 1999. Interaction of cholesterol with sphingomyelins and acyl-chain-matched phosphatidylcholines: a comparative study of the effect of the chain length. *Biophys. J.* 76:908–915.
18. Kuikka, M., B. Ramstedt, …, J. P. Slotte. 2001. Membrane properties of D-erythro-N-acyl sphingomyelins and their corresponding dihydro species. *Biophys. J.* 80:2327–2337.
19. Epand, R. M. 2003. Cholesterol in bilayers of sphingomyelin or dihydrosphingomyelin at concentrations found in ocular lens membranes. *Biophys. J.* 84:3102–3110.
20. Nyholm, T., M. Nylund, …, J. P. Slotte. 2003. Properties of palmitoyl phosphatidylcholine, sphingomyelin, and dihydrosphingomyelin bilayer membranes as reported by different fluorescent reporter molecules. *Biophys. J.* 84:987–997.
21. Nyholm, T. K., M. Nylund, and J. P. Slotte. 2003. A calorimetric study of binary mixtures of dihydrosphingomyelin and sterols, sphingomyelin, or phosphatidylcholine. *Biophys. J.* 84:3138–3146.
22. Yasuda, T., M. A. Al Sazzad, …, J. P. Slotte. 2016. The influence of hydrogen bonding on sphingomyelin/colipid interactions in bilayer membranes. *Biophys. J.* 110:431–440.
23. Parasassi, T., G. De Stasio, …, E. Gratton. 1991. Quantitation of lipid phases in phospholipid vesicles by the generalized polarization of Laurdan fluorescence. *Biophys. J.* 60:179–189.
24. De Vequi-Suplicy, C. C., C. R. Benatti, and M. T. Lamy. 2006. Laurdan in fluid bilayers: position and structural sensitivity. *J. Fluoresc.* 16:431–439.
25. Bagatolli, L. A., T. Parasassi, …, E. Gratton. 1999. A model for the interaction of 6-lauroyl-2-(N,N-dimethylamino)naphthalene with lipid environments: implications for spectral properties. *Photochem. Photobiol.* 70:557–564.

26. Parasassi, T., E. K. Krasnowska, …, E. Gratton. 1998. Laurdan and prodan as polarity-sensitive fluorescent membrane probes. *J. Fluoresc.* 8:365–373.

27. Vequi-Suplicy, C. C., K. Coutinho, and M. T. Lamy. 2014. Electric dipole moments of the fluorescent probes Prodan and Laurdan: experimental and theoretical evaluations. *Biophys. Rev.* 6:63–74.

28. Parasassi, T., G. De Stasio, …, E. Gratton. 1990. Phase fluctuation in phospholipid membranes revealed by Laurdan fluorescence. *Biophys. J.* 57:1179–1186.

29. Parasassi, T., E. Gratton, …, M. Levi. 1997. Two-photon fluorescence microscopy of laurdan generalized polarization domains in model and natural membranes. *Biophys. J.* 72:2413–2429.

30. Harris, F. M., K. B. Best, and J. D. Bell. 2002. Use of laurdan fluorescence intensity and polarization to distinguish between changes in membrane fluidity and phospholipid order. *Biochim. Biophys. Acta.* 1565:123–128.

31. Bacalum, M., B. Zorilă, and M. Radu. 2013. Fluorescence spectra decomposition by asymmetric functions: Laurdan spectrum revisited. *Anal. Biochem.* 440:123–129.

32. Malacrida, L., S. Astrada, …, L. A. Bagatolli. 2016. Spectral phasor analysis of LAURDAN fluorescence in live A549 lung cells to study the hydration and time evolution of intracellular lamellar body-like structures. *Biochim. Biophys. Acta.* 1858:2625–2635.

33. Jay, A. G., and J. A. Hamilton. 2017. Disorder amidst membrane order: standardizing laurdan generalized polarization and membrane fluidity terms. *J. Fluoresc.* 27:243–249.

34. Massey, J. B. 2001. Interaction of ceramides with phosphatidylcholine, sphingomyelin and sphingomyelin/cholesterol bilayers. *Biochim. Biophys. Acta.* 1510:167–184.

35. Hope, M. J., M. B. Bally, …, P. R. Cullis. 1985. Production of large unilamellar vesicles by a rapid extrusion procedure: characterization of size distribution, trapped volume and ability to maintain a membrane potential. *Biochim. Biophys. Acta.* 812:55–65.

36. Rouser, G., S. Fkeischer, and A. Yamamoto. 1970. Two dimensional then layer chromatographic separation of polar lipids and determination of phospholipids by phosphorus analysis of spots. *Lipids.* 5:494–496.

37. Haugland, R. P. 1996. Handbook of Fluorescent Probes and Research Chemicals, Sixth Edition. Molecular Probes Inc, Eugene, OR.

38. Lakowicz, J. R. 1999. Principles of Fluorescence Spectroscopy. Kluvert Academic/Plenum Publishers, New York.

39. Mohana-Borges, R., J. Lima Silva, and G. de Prat-Gay. 1999. Protein folding in the absence of chemical denaturants. Reversible pressure denaturation of the noncovalent complex formed by the association of two protein fragments. *J. Biol. Chem.* 274:7732–7740.

40. Parasassi, T., G. Ravagnan, …, E. Gratton. 1993. Modulation and dynamics of phase properties in phospholipid mixtures detected by Laurdan fluorescence. *Photochem. Photobiol.* 57:403–410.

41. Viard, M., J. Gallay, …, M. Paternostre. 1997. Laurdan solvatochromism: solvent dielectric relaxation and intramolecular excited-state reaction. *Biophys. J.* 73:2221–2234.

42. Józefowicz, M., K. A. Kozyra, …, J. Heldt. 2005. Effect of hydrogen bonding on the intramolecular charge transfer fluorescence of 6-dodecanoyl-2-dimethylaminonaphtalene. *Chem. Phys.* 320:45–53.

43. Cevc, G. 1990. Membrane electrostatics. *Biochim. Biophys. Acta.* 1031:311–382.

44. Gramse, G., A. Dols-Perez, …, G. Gomila. 2013. Nanoscale measurement of the dielectric constant of supported lipid bilayers in aqueous solutions with electrostatic force microscopy. *Biophys. J.* 104:1257–1262.

45. Coster, H. G. L., T. C. Chilcott, and A. C. F. Coste. 1996. Impedance spectroscopy of interfaces, membranes and ultrastructures. *Bioelectrochem. Bioenerg.* 40:79–98.

46. Ferguson-Yankey, S. R., D. Borchman, …, M. C. Yappert. 2000. Conformational studies of sphingolipids by NMR spectroscopy. I. Dihydrosphingomyelin. *Biochim. Biophys. Acta.* 1467:307–325.

47. Talbott, C. M., I. Vorobyov, …, M. C. Yappert. 2000. Conformational studies of sphingolipids by NMR spectroscopy. II. Sphingomyelin. *Biochim. Biophys. Acta.* 1467:326–337.

48. Kinoshita, M., N. Matsumori, and M. Murata. 2014. Coexistence of two liquid crystalline phases in dihydrosphingomyelin and dioleoylphosphatidylcholine binary mixtures. *Biochim. Biophys. Acta.* 1838:1372–1381.

49. Griffin, R. G., L. Powers, and P. S. Pershan. 1978. Head-group conformation in phospholipids: a phosphorus-31 nuclear magnetic resonance study of oriented monodomain dipalmitoylphosphatidylcholine bilayers. *Biochemistry.* 17:2718–2722.

50. Büldt, G., H. U. Gally, …, G. Zaccai. 1979. Neutron diffraction studies on phosphatidylcholine model membranes. I. Head group conformation. *J. Mol. Biol.* 134:673–691.

51. Gally, H. U., W. Niederberger, and J. Seelig. 1975. Conformation and motion of the choline head group in bilayers of dipalmitoyl-3-sn-phosphatidylcholine. *Biochemistry.* 14:3647–3652.

52. Chattopadhyay, A., and E. London. 1987. Parallax method for direct measurement of membrane penetration depth utilizing fluorescence quenching by spin-labeled phospholipids. *Biochemistry.* 26:39–45.

53. Abrams, F. S., and E. London. 1993. Extension of the parallax analysis of membrane penetration depth to the polar region of model membranes: use of fluorescence quenching by a spin-label attached to the phospholipid polar headgroup. *Biochemistry.* 32:10826–10831.

54. Cevc, G. 1987. How membrane chain melting properties are regulated by the polar surface of the lipid bilayer. *Biochemistry.* 26:6305–6310.

55. Lakowicz, J. R., and A. Balter. 1982. Analysis of excited-state processes by phase-modulation fluorescence spectroscopy. *Biophys. Chem.* 16:117–132.

56. Lakowicz, J. R., and A. Balter. 1982. Differential-wavelength deconvolution of time-resolved fluorescence intensities. A new method for the analysis of excited-state processes. *Biophys. Chem.* 16:223–240.

57. Rowe, B. A., C. A. Roach, …, S. L. Neal. 2008. Spectral heterogeneity of PRODAN fluorescence in isotropic solvents revealed by multivariate photokinetic analysis. *J. Phys. Chem. A.* 112:13402–13412.

58. Vequi-Suplicy, C. C., K. Coutinho, and M. T. Lamy. 2015. New insights on the fluorescent emission spectra of Prodan and Laurdan. *J. Fluoresc.* 25:621–629.

Biophysical Journal, Volume *116*

Supplemental Information

Solvatochromic Modeling of Laurdan for Multiple Polarity Analysis of Dihydrosphingomyelin Bilayer

Nozomi Watanabe, Yuka Goto, Keishi Suga, Thomas K.M. Nyholm, J. Peter Slotte, and Hiroshi Umakoshi

Emission spectra of Laurdan in DOPC/PSM and DOPC/DHPSM bilayer

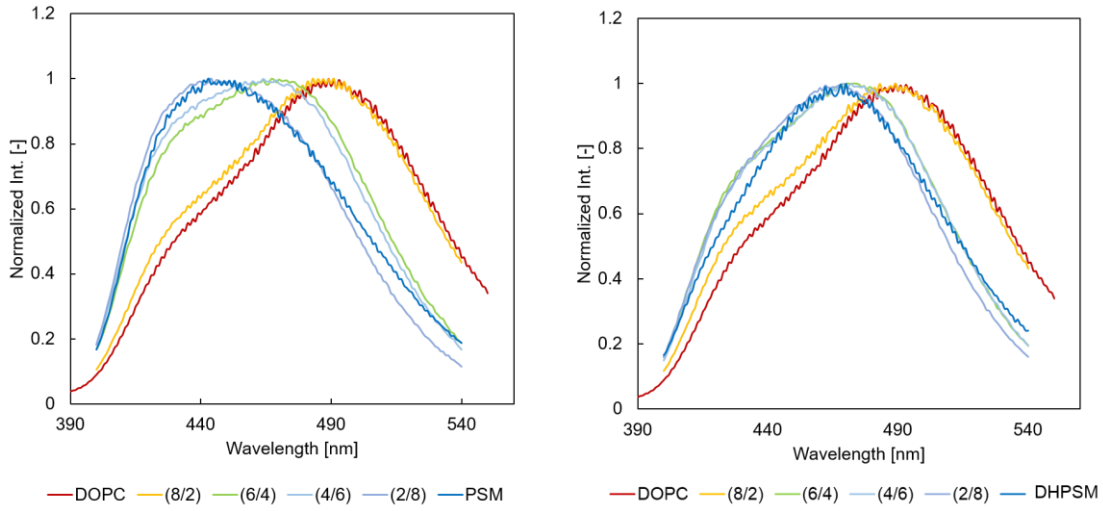

Figure S1. Fluorescence emission spectra of Laurdan in the DOPC/PSM and DOPC/DHPSM binary systems at 20 °C. The ratios of the lipid composition of DOPC, PSM, and DHPSM are written as (DOPC/PSM (or DHPSM)). The excitation wavelength is 360 nm. All spectra were normalized with the strongest peak intensity. The reproducibility was confirmed from the transition as a function of lipid composition.

Transition of the *GP* value

The generalized polarization value was measured according to a previous report (1) with the following equation:

$$GP = \frac{I_{440\ \mathrm{nm}} - I_{490\ \mathrm{nm}}}{I_{440\ \mathrm{nm}} + I_{490\ \mathrm{nm}}} \qquad \text{(Eq. S1)}$$

where $I_{440\ \mathrm{nm}}$ is the emission intensity at 440 nm in the emission spectrum of Laurdan in the steady state, and $I_{490\ \mathrm{nm}}$ is the emission intensity at 490 nm.

The *GP* values decreased with an increase in temperature. Except for DOPC, the values shifted drastically based on the transition temperature. At room temperature, *GP* values become smaller in the order of DPPC > PSM > DHPSM > DOPC, which also corresponds to the order of degree of hydration.

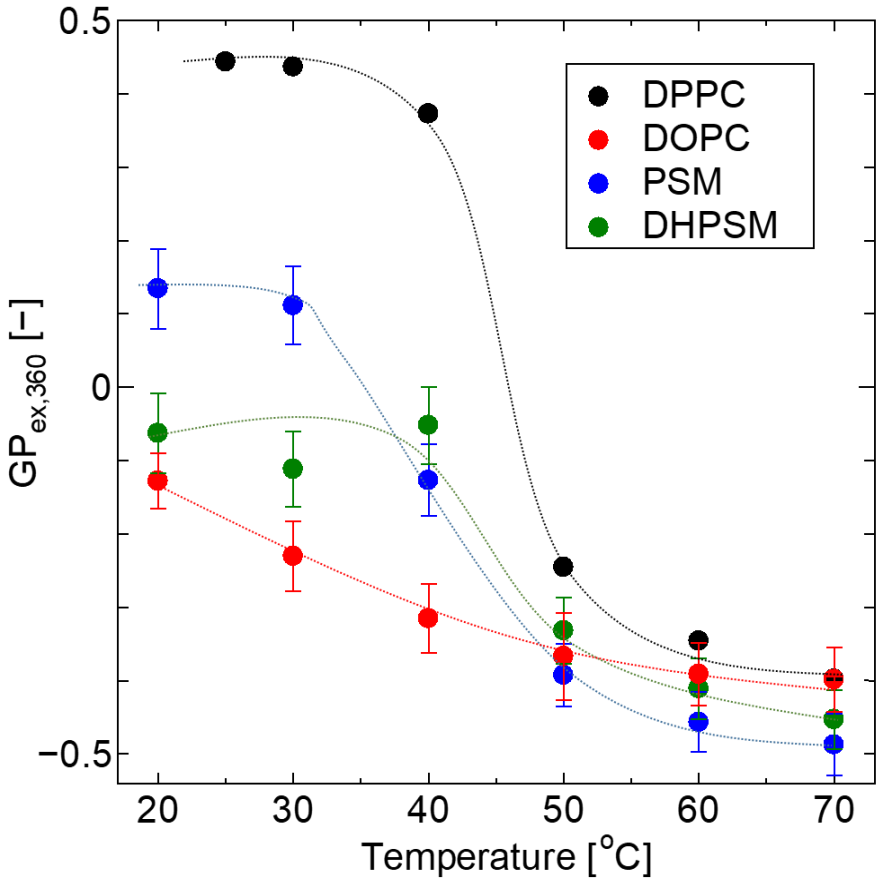

Figure S2. Transition of *GP* values in the DPPC, DOPC, PSM, and DHPSM bilayers as a function of temperature. Each lipid is depicted in the color described in the legends. The *GP* value is defined as described in Eq. S1. The average value was plotted from the *GP* values calculated from the three emission spectra shown in Figure 1. Error bars represent SEM.

Anisotropy of Laurdan in binary bilayers

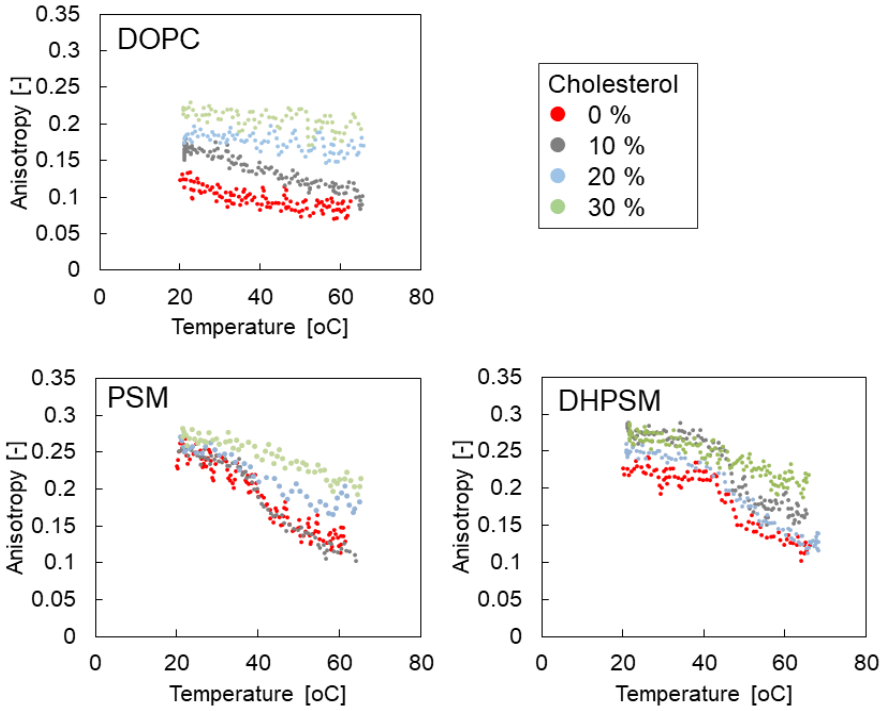

Figure S3. Anisotropy transition of Laurdan as a function of temperature observed in DOPC/cholesterol, PSM/cholesterol, and DHPSM/cholesterol binary bilayer systems. Red curves represent single component lipid bilayers, DOPC, PSM, and DHPSM, respectively. The legend shows the composition of cholesterol. The excitation wavelength were 360 nm and 490 nm for the emission. Anisotropy was measured as described in the Methods section using the Eq. 1 and 2. The reproducibility was confirmed from the transition as a function of temperature. For all samples, a large scattering was observed in the anisotropy values, which could be due to the variety of orientations in each molecular environment where Laurdan exists.

Quenching experiment with 5-DOXYL and TEMPO

Fluorescence quenching experiments were performed to reveal the multiplicity of Laurdan locations in DPPC, DOPC, PSM, and DHPSM bilayers. The spin-labeled quenchers 2-(3-carboxypropyl)4,4-dimethyl-2-tridecyl-3-oxazolidinyloxy (5-DOXYL stearic acid) and 2,2,6,6-tetramethylpiperidine 1-oxyl free radical (TEMPO) were used as a site-specific quencher and bulk-distributed quencher, respectively. According to the parallax method using l-palmitoyl-2-(5-doxyl)stearoyl-*sn*-glycero-3-phosphocholine, the distance from the bilayer center to the 5-DOXYL moiety in stearoyl chain is estimated to be 12.15 Å in DOPC bilayer (2, 3). The fluorescence would be quenched if the Laurdan molecules were located as close as they are to the radical molecules. TEMPO is a water-soluble molecule and is partitioned favorably into the disordered phase of the lipid membrane. Therefore, the penetration of TEMPO and quenching would be promoted as the increase of TEMPO concentration.

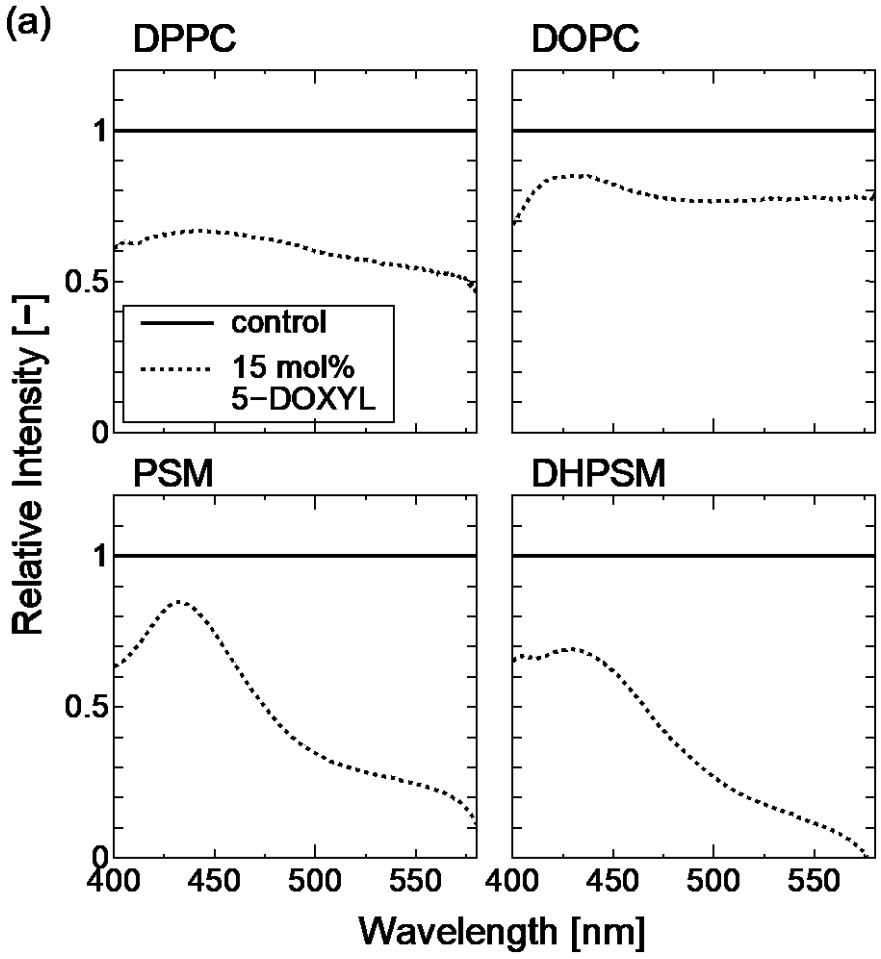

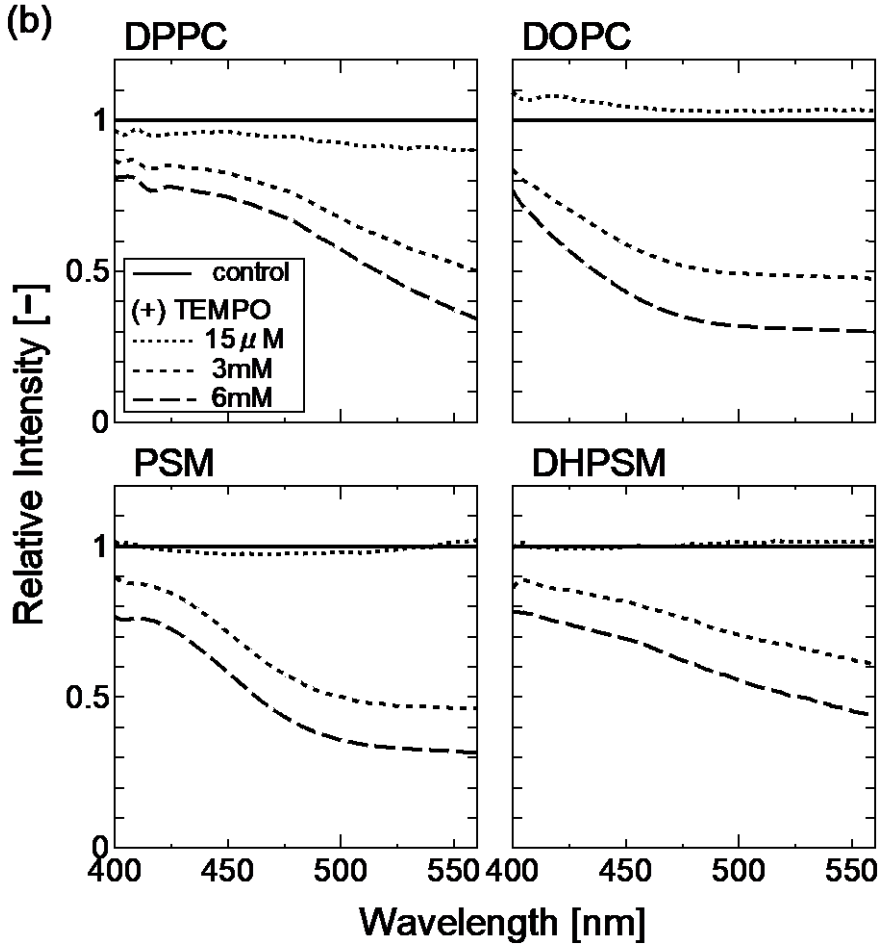

Figure S4. Relative emission intensity of Laurdan in the presence of quenchers, shown as a spectrum. The solid lines represent the emission spectra of Laurdan as a control, and the dotted lines represent the relative intensities between the spectra obtained **(a)** in the presence of 15 mol% of 5-DOXYL stearic acid and **(b)** in the presence of TEMPO. All experiments were performed with a 100-μM lipid concentration and 3 mol% of Laurdan, respectively. The emission spectra were obtained with excitation at 360 nm at 20 °C. All spectra acquisitions were repeated three times.

Center of mass of time-resolved emission spectra of Laurdan

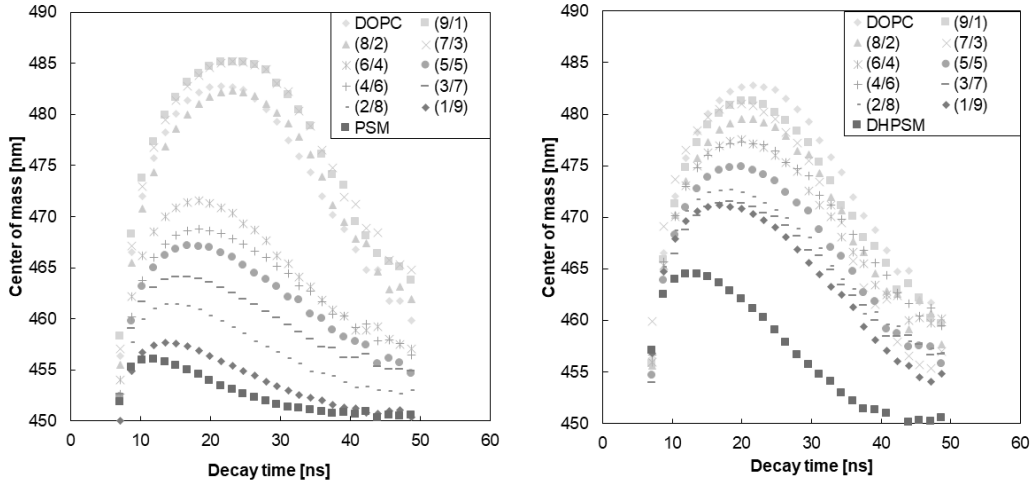

Figure S5. Center of spectral mass for each bilayer in the DOPC/PSM and DOPC/DHPSM binary systems at 20°C. The ratios of the lipid composition of DOPC, PSM, or DHPSM are written as (DOPC/PSM (or DHPSM)). The excitation wavelength of the pus laser is 378 nm. The value was calculated according to Eq. 4, and data points were extracted every 7.168 ns. The composition of PSM or DHPSM is increasing as the color gets darker. The reproducibility was confirmed from the transition as a function of lipid composition.

Excitation spectra of Laurdan

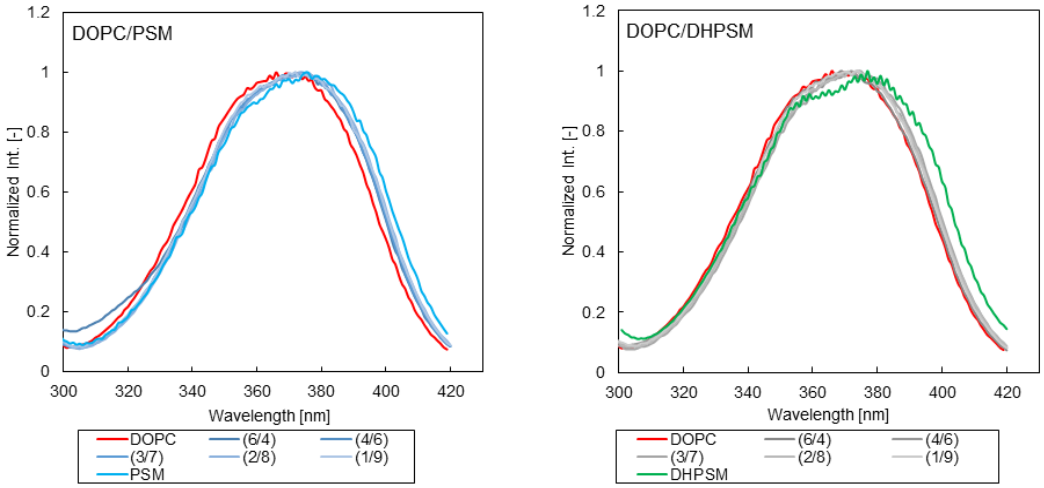

Figure S6. Excitation spectra of Laurdan in DOPC/PSM and DOPC/DHPSM bilayers, recorded at the emission wavelength of λ_{em} = 435 nm at 20 °C. The ratios of the bilayer lipids composition of DOPC, PSM or DHPSM are written in (DOPC/PSM (or DHPSM)). DOPC, PSM, and DHPSM are illustrated in the color of red, blue and green, respectively. The intermediate composition is represented by the gradient of color. All spectra were normalized with the strongest peak intensity. The reproducibility was confirmed from the transition as a function of lipid composition.

Excitation dependencies in the emission spectra

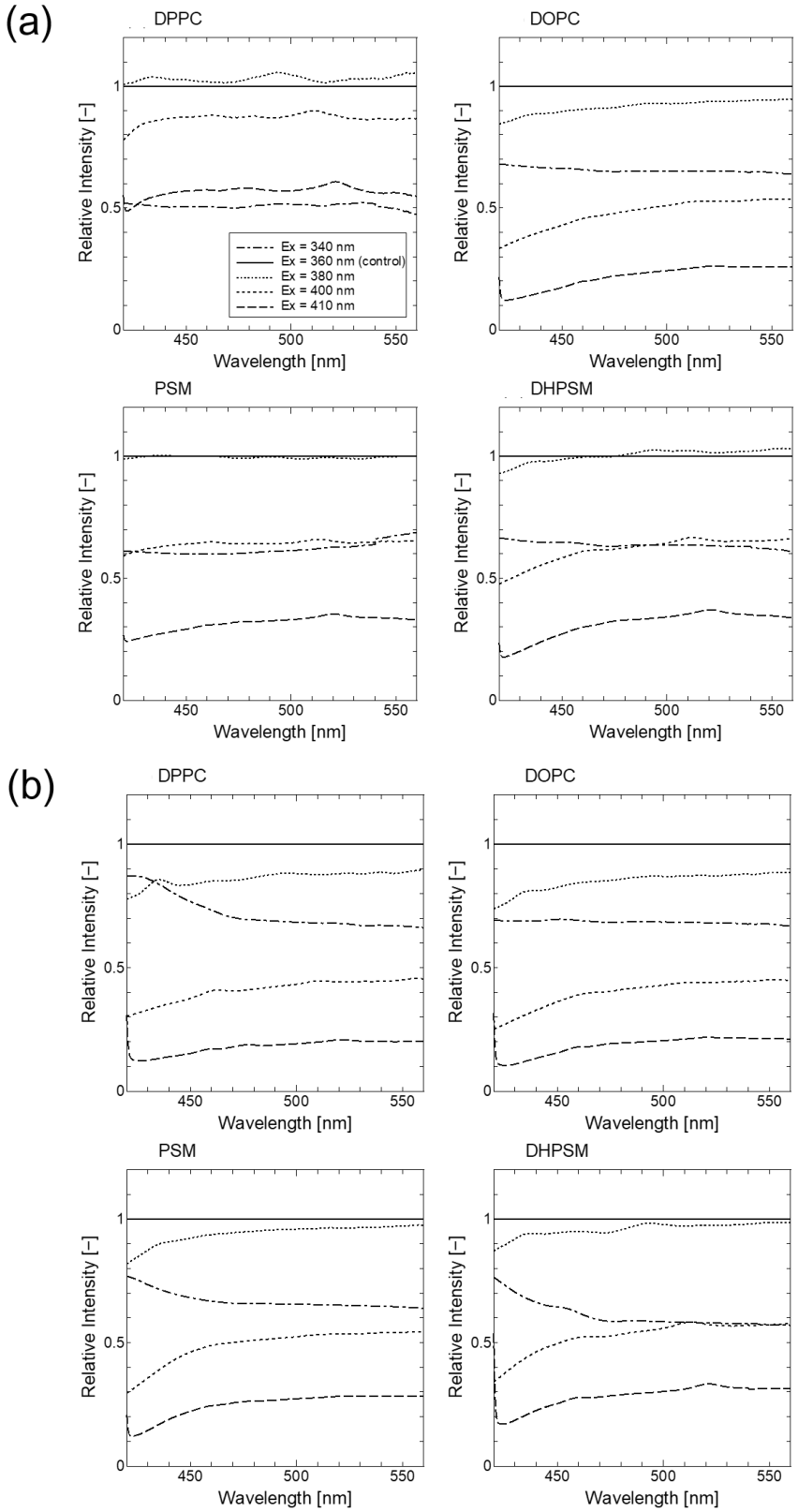

Figure S7. Ratio spectra between steady-state Laurdan emission spectra excited at various

excitation wavelengths. The results were obtained (a) at 25 °C and (b) at 60 °C. All spectra were calculated with the spectra excited at 360 nm as a control. The arbitrary excitation wavelengths are shown in the legend. The concentrations of samples were 100 μM of lipids and 1 mol % of Laurdan, respectively. All spectra acquisitions were repeated three times.

Deconvolution analysis and the solvent model

The fitting parameters were carefully selected based on considerations related to mixed solvent systems. First, a deconvolution analysis was performed as follows:

1. The second-derivative approach was performed to get the candidate peaks.
2. The asymmetric fitting equation was used for the deconvolution following a previous report (4).
3. Peaks with relative areas under curve of less than 3 % was regarded as making no contribution to the entire spectrum and were eliminated.
4. Some candidate peaks were selected from those with the highest R^2 values.

Consequently, the fitting parameters for the solvent systems were obtained empirically, such as the number of components in the solvent system, the peak positions, and the full width at half maximum (FWHM). The dielectric constants of each solvent system were measured using a dielectric probe kit (Model 85070C and a PNA-L Network Analyzer Model N5230C from Agilent Technologies, Santa Clara, CA, USA).

The deconvolution in the mixed system of acetone–hexane, hexane-ethanol, and ethanol–water were calculated with single or double fitting components. A comparison of the R^2 values of the single and double component deconvolutions are shown in Figure S8.

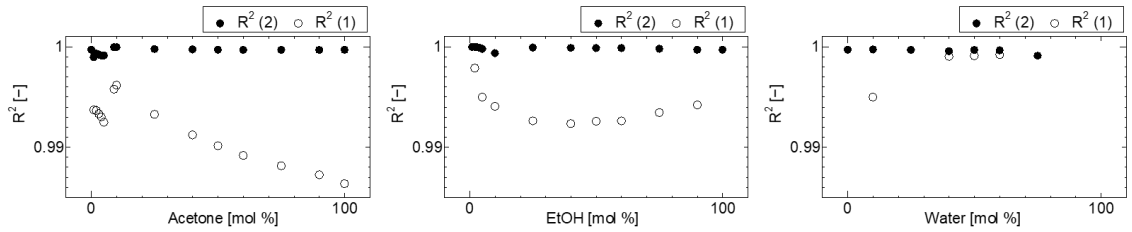

Figure S8. Comparison of the R^2 values in the acetone–hexane (left), hexane-ethanol (middle), and ethanol–water (right) systems. The R^2 values deconvoluted with two components and single components are represented as R^2 (2) and R^2 (1), as shown in the legend, respectively.

According to the higher R^2 values of deconvolutions with two components in Figure S8, the results obtained with two-component deconvolution fitting were discussed. The peak position and the FWHM of each component are summarized in Figure S9. Each point corresponds to the plot shown in Figure S10.

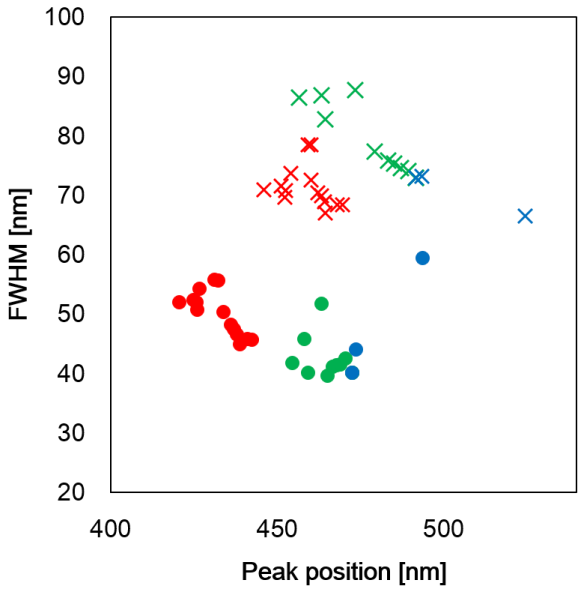

Figure S9. Summary of the correlation between emission peak position and FWHM for each deconvoluted peak. Red: hexane–acetone system; green: hexane–ethanol system; blue: ethanol–water system. The main deconvolution components are represented by filled circles, and the relaxed components were marked with crosses.

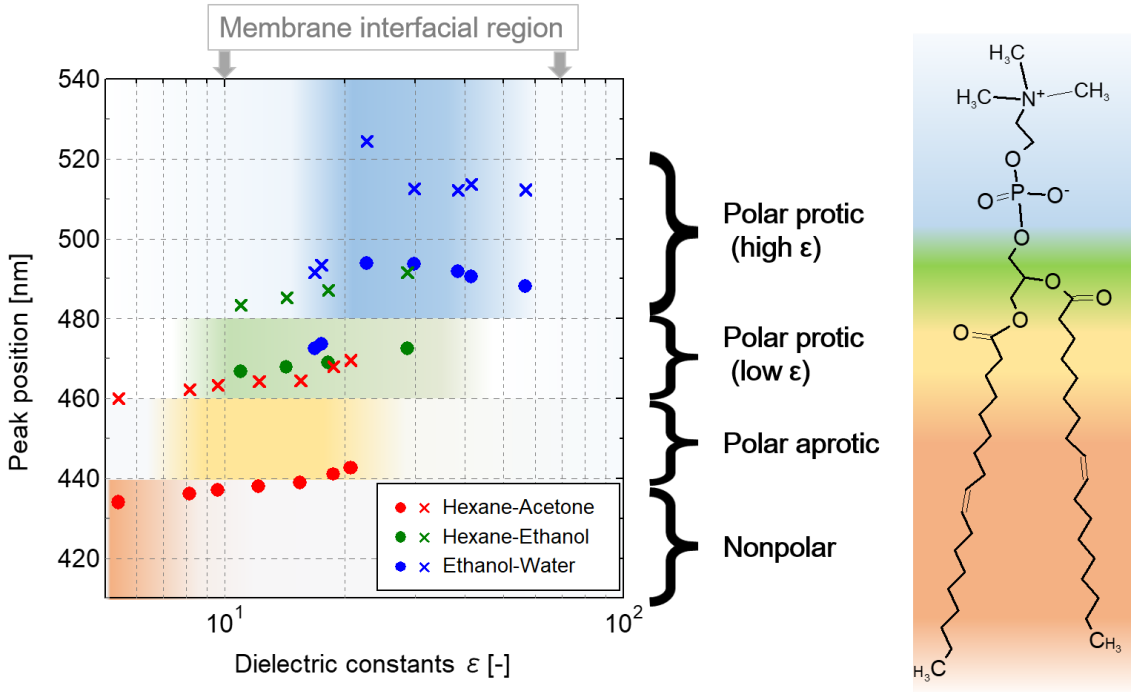

Figure S10. (Left) Correlation between the dielectric constants and the deconvoluted peak position. Red: hexane–acetone system; green: hexane–ethanol system; blue: ethanol–water system. The main deconvolution components are represented by filled circles, and the relaxed components are marked with crosses. The dielectric constants (ε) were measured using a dielectric probe kit. The interfacial region of the membrane was colored in the corresponding ε values (ε; 10 ~ 70), as reported previously (5). (Right) Chemical structure and corresponding dielectric constants for DOPC, according to the schematic diagram for egg PC (6).

The correlation between the emission peak and the dielectric constants and emission peak positions were red-shifted in the following order: hexane–acetone, hexane–ethanol, and ethanol–water (Figure S10). The shifts of peak position as a function of the dielectric constant indicated similar dependencies in any solvent system. The peak positions were stable with a wide range of dielectric constants. The two components found in a solvent system showed different FWHM values, and the one component with larger FWHM had a longer emission wavelength compared with another component (Figure S9). This broad and red-shifted component could be found even at a very low dielectric constant ($\varepsilon < 5$), indicating that this component was in a relaxed state not only because of the solvent but also due to undefined environmental factors, such as heat, collision, and reorientation. Laurdan and Prodan have two excitation states in a homogeneous solvent system, as suggested by the existence of two

lifetimes (7–9). Hence, the deconvolution with two components in a solvent system is consistent with previous finding (10).

The deconvolution of Laurdan spectra in the lipid bilayer was performed using the same procedure for solvent systems explained previously. After deconvolution, four types of peak positions were finally resulted from all of lipid bilayer systems through the temperature ranges tested in this work (Figure 5B), wherein the peaks 1, 2, 3 and 4 were observed at less than 440 nm, 440 ~ 460 nm, 460 ~ 480 nm and greater than 480 nm, respectively. The values of peak position and FWHM observed in the solvent system serve as reference boundaries for the peak positions ($420 < \lambda < 540$ nm) and FWHM ($30 < FWHM < 90$ nm), respectively (Figure S9). FWHM values for the deconvolution results in lipid bilayers are shown in Figure S11. These results suggest that the deconvoluted components of Laurdan spectra in lipid bilayers can be assigned to those in solvent systems. The number of components was changed from four to three when the R^2 value of the deconvolution with three components reached the value of the deconvolution with four components in the trial. Moreover, the amplitude of the first component located at the shorter wavelength was small to negligible. Most of the obtained spectra showed that the value of the asymmetry at half-maximum was approximately 1, which indicates that most of the deconvolution spectra were nearly symmetrical. The deconvolution based on the solvent model can be explained with the symmetric Gaussian function (10). The procedure for the deconvolution analysis is summarized in Scheme 1.

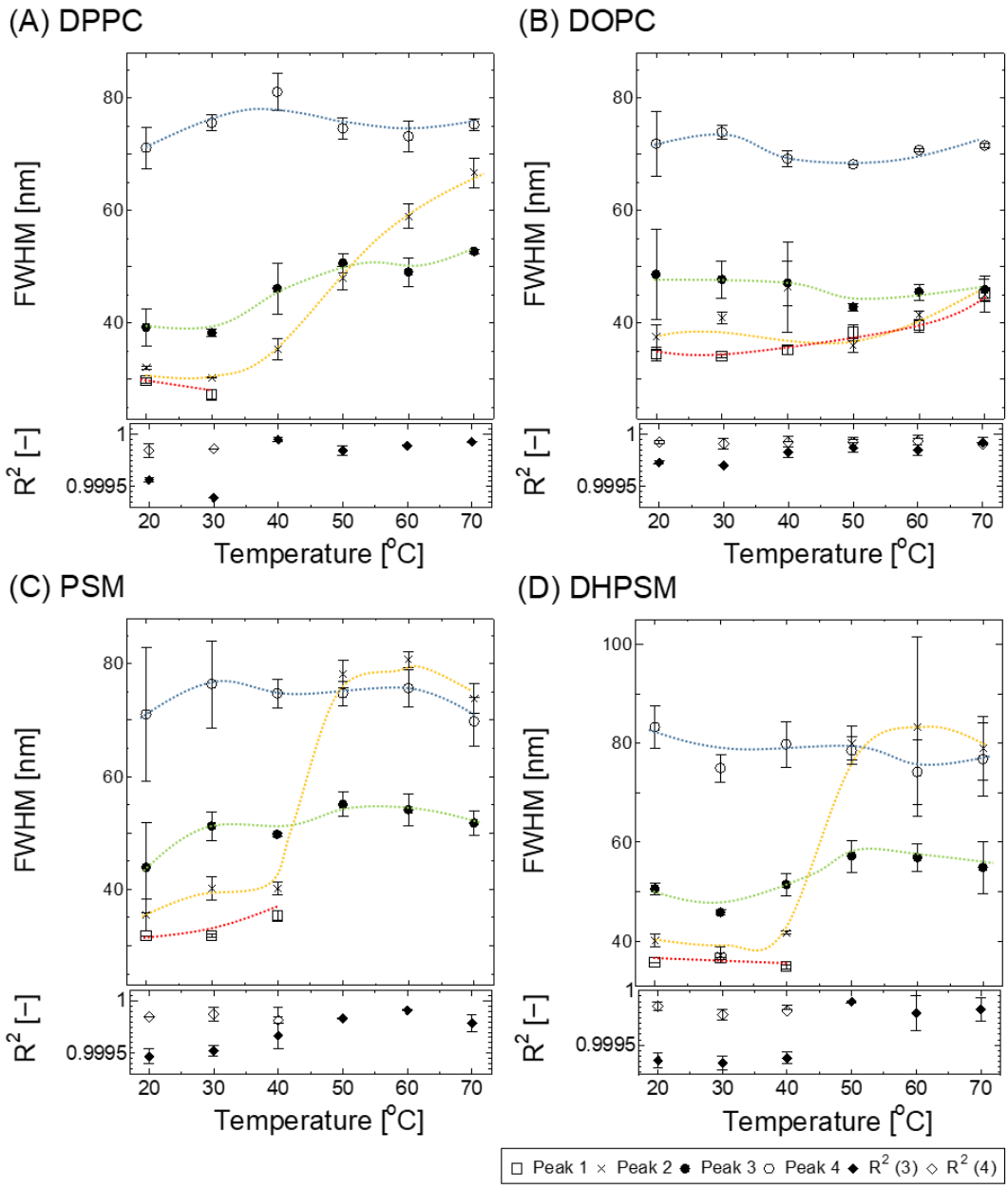

Figure S11. Summary of the FWHM of deconvolution results in lipid bilayers: (A) DPPC, (B) DOPC, (C) PSM, and (D) DHPSM. The red, yellow, green, and blue lines correspond to the components of the nonpolar (Peak 1), the polar aprotic (Peak 2), the polar protic with low ε (Peak 3), and the polar protic with high ε (Peak 4), respectively. The R^2 values are shown in each bottom panel. Solid diamonds represent R^2 values analyzed with three deconvolution curves, and open diamonds represent those analyzed with four curves, respectively. Error bars represent SEM.

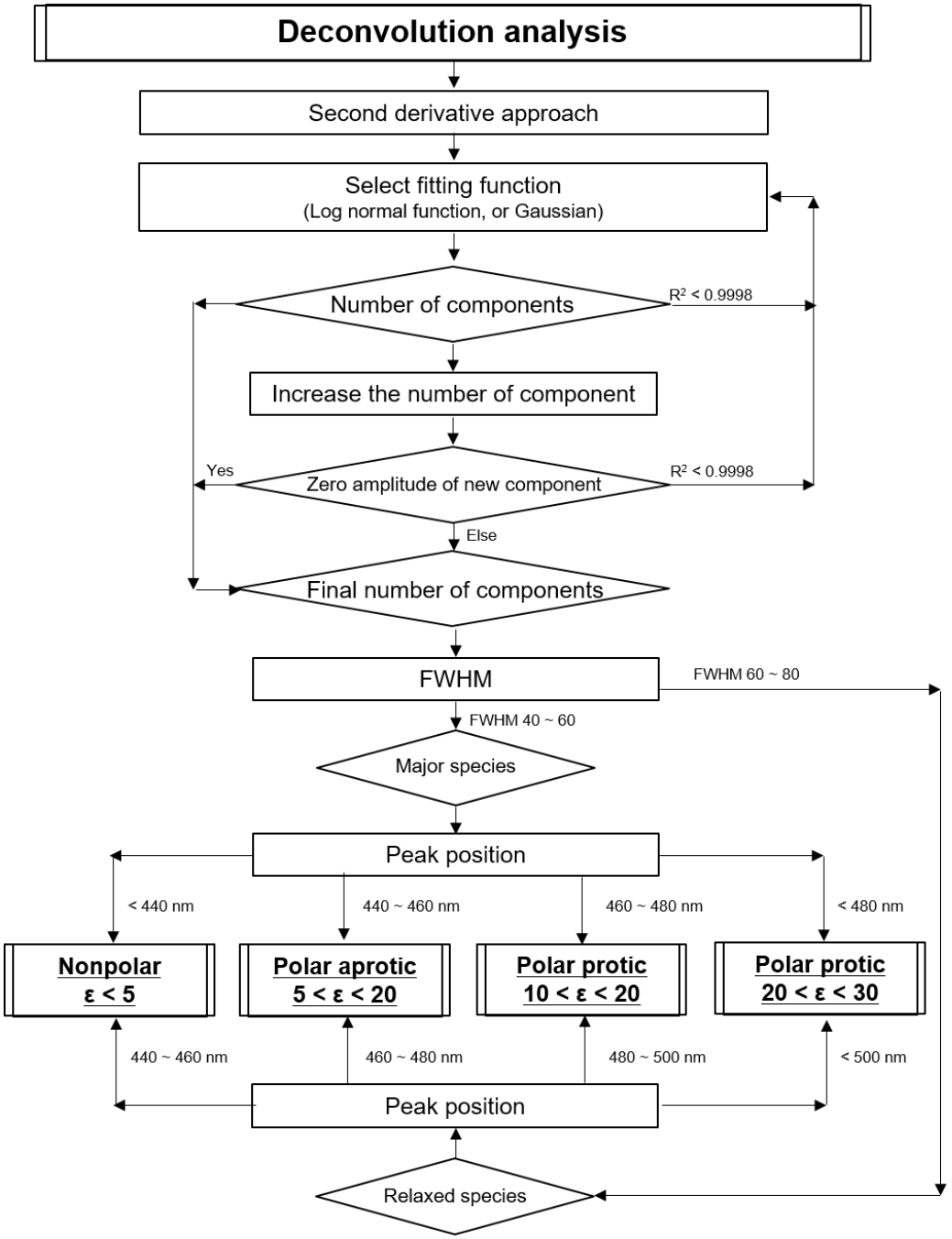

Scheme 1. Deconvolution analysis procedure.

Plausible molecular model above T_m

The molecular model relations above T_m are illustrated. Since the fluorescence behavior observed after phase transition was similar in the DPPC, PSM, and DHPSM bilayers, the model could be illustrated as shown below.

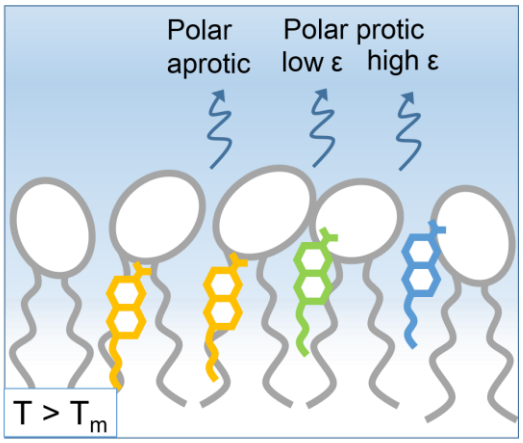

Figure S12. Molecular model above T_m for the DPPC, PSM, and DHPSM bilayers. The colors of the Laurdan are illustrated with the corresponding color in Figure 5: yellow for the polar aprotic, green for the polar protic with low ε, and blue for the polar protic with high ε.

Supporting References

1. Parasassi, T., G. De Stasio, G. Ravagnan, R.M. Rusch, and E. Gratton. 1991. Quantitation of lipid phases in phospholipid vesicles by the generalized polarization of Laurdan fluorescence. Biophys. J. 60: 179–189.

2. Chattopadhyay, A., and E. London. 1987. Parallax method for direct measurement of membrane penetration depth utilizing fluorescence quenching by spin-labeled phospholipids. Biochemistry. 26: 39–45.

3. Abrams, F.S., and E. London. 1993. Extension of the parallax analysis of membrane penetration depth to the polar region of model membranes: Use of fluorescence quenching by a spin-label attached to the phospholipid polar headgroup. Biochemistry. 32: 10826–10831.

4. Bacalum, M., B. Zorilă, and M. Radu. 2013. Fluorescence spectra decomposition by asymmetric functions: Laurdan spectrum revisited. Analytical Biochemistry. 440: 123–129.

5. Cevc, G. 1987. How membrane chain melting properties are regulated by the polar surface of the lipid bilayer. Biochemistry. 26: 6305–6310.

6. Coster, H.G.L., T.C. Chilcott, and A.C.F. Coste. 1996. Impedance spectroscopy of interfaces, membranes and ultrastructures. Bioelectrochem Bioenerg. 40: 79–98.

7. Lakowicz, J.R., and A. Balter. 1982. Analysisofexcited-state processes by phase-modulation fluorescence spectroscopy. Biophys. Chem. 16: 117–132.

8. Lakowicz, J.R., and A. Balter. 1982. Differential-wavelength deconvolution of time-resolved fluorescence intensities - a new method for the analysis of excited-state processes. Biophys. Chem. 16: 223–240.

9. Rowe, B.A., C.A. Roach, J. Lin, V. Asiago, O. Dmitrenko, and S.L. Neal. 2008. Spectral Heterogeneity of PRODAN Fluorescence in Isotropic Solvents Revealed by Multivariate Photokinetic Analysis. The Journal of Physical Chemistry A. 112: 13402–13412.

10. Vequi-Suplicy, C.C., K. Coutinho, and M.T. Lamy. 2015. New Insights on the Fluorescent Emission Spectra of Prodan and Laurdan. Journal of Fluorescence. 25: 621–629.